CHEMISTRY OF MATERIALS

Article

pubs.acs.org/cm

Are Two Azo Groups Better than One? Investigating the Photoresponse of Polymer-Bisazobenzene Complexes

Jaana Vapaavuori,*[,†,‡,∥] Alexis Goulet-Hanssens,*[,§,⊥,∥] Ismo T.S. Heikkinen,[†] Christopher J. Barrett,[§] and Arri Priimagi[†,#]

[†]Department of Applied Physics, Aalto University, P. O. Box 13500, FI-00076 Aalto, Finland

[‡]Department of Chemistry, University of Montreal, C.P. 6128, Succursale Centre-Ville, Montreal, Quebec H3C 3J7, Canada

[§]Department of Chemistry, McGill University, 801 Sherbrooke Street West, Montreal, Quebec H3A 0B8, Canada

ABSTRACT: Azobenzene chromophores are an ideal choice for material applications where functionality needs to be activated in a precise remote-controlled fashion. The azobenzene stimuli-response falls into two categories, either based on efficient *trans*-to-*cis* photoisomerization and a high *cis* yield enabling on−off type functions, or relying on a fast *trans*−*cis*−*trans* cycling creating motion in the material system. Herein, we show that using bisazochromophores instead of the more common monoazobenzene derivatives makes a difference in the performance of light-responsive azopolymers, more specifically in photo-orientation and all-optical surface patterning. Our findings point out that polymer-bisazobenzene complexes are an attractive alternative as high-performance photoreponsive materials and that although their properties are highly sensitive to the extent of conjugation in the system, they can be designed into relatively transparent films with high performance for all-optical patterning.

Which switch better patterns polymers?

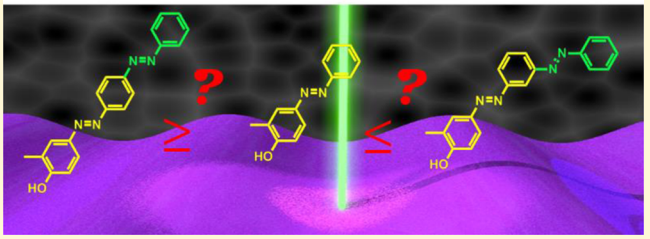

INTRODUCTION

Stimuli-response is a critical feature in many smart materials,[1] and light is the best suited stimulus to deliver a localized, dosed input with high spatiotemporal control. Azobenzene has been extremely prevalent in the literature as a reliable, reusable photoswitch that can affect large molecular and macromolecular changes upon irradiation with light.[2,3] Azobenzene's reversible *trans*−*cis* photoisomerization yields a *cis* state that is metastable and will thermally reconvert to the *trans* state. Functionalizing polymers with these chromophores provides materials with interesting surface- as well as bulk-switching properties.[4,5] Chromophore incorporation can be achieved through various means, either by covalently linking the chromophores to the polymer chain, doping them in the system or making use of supramolecular interactions to localize the azobenzene molecules.[6] To optimize the light-triggered work of azo materials, both the chromophores and their attachment to a system need to be designed to optimize their desired function.

Achieving successful light-response in materials can rely either on a system that can attain a high photostationary state (light pushing a chromophore to an "on"/"off" state) or rapid cycling between isomers to drive material response (light activating a material system to an "on" state).[4,7−9] Remarkable changes in materials properties can be observed, even if the extent of isomerization is heavily hindered. For instance, crystals of pure azobenzenes, bearing an ultrahigh optical density can be bent with light.[10,11] Likewise, brush architectures and liquid-crystalline assemblies having large chromophore content can be switched to impart large macromolecular deformations in films,[12,13] long-range ordering in liquid crystalline environments,[14−18] and changes to chirality.[19,20] This demonstrates that one can still engineer systems exhibiting large material changes with classically suboptimal isomerization conditions. Controlling material properties using photoinduced motions driven by *trans*−*cis*−*trans* cycling is of interest for fabricating dynamic photomechanical materials, such as light-powered oscillators,[21] and for the inscription of light-induced surface-relief gratings (SRGs) for photonics and nanostructuring applications.[22] Improving both types of switching is highly desired, and a comprehensive understanding on the connections between the azo chromophore, their environment, and the efficiency of photoinduced phenomena is critical for effective use of azobenzene systems in materials applications.

Polyconjugated azobenzenes have been used as dyes that have a potential to achieve larger light-induced molecular changes than an individual chromophore. These polyazos can achieve a high *cis* content if they are electronically decoupled either by adding in a twist angle between neighboring dyes[7,23] to prevent conjugation in the system, or changing the position of polyazobenzene from a *para*−*para* orientation to a *para*−*meta*.[24] In addition to loading more isomerizing units into a material without aggregation, bisazo architectures can provide larger volume change upon isomerization and the possibility to separately address both azo groups[25] compared to monoazos.

Received: June 26, 2014
Revised: August 14, 2014
Published: August 18, 2014

Although polyazo chromophores are extremely interesting as drivers for photoinduced motions, there are few systematic studies on the structure−property relations in bisazo systems. Meng and co-workers demonstrated the importance of using bisazochromophores in photo-orientation,[26] and Wang and co-workers made an extensive structure−property study of all-optical surface patterning,[27] both using covalent azopolymers bearing bisazochromophore pendant units in the side chains. In 2010, using supramolecular hydrogen-bonded polyazo complexes, Wu and co-workers reported on high and stable birefringence values upon hydrogen bonding of an azo dye to the side-chain of a polymer already containing an azo unit.[28] The same year, bisazobenzene complexes hydrogen-bonded directly to a poly(4-vinylpyridine) (p4VP) polymer backbone being capable for efficient SRG formation were introduced,[29] followed by optimization of the hydrogen-bonded bisazobenzene chromophore, affording SRGs that can be inscribed over large range of wavelengths.[30]

Exactly how bisazo chromophores affect material changes remains unclear, as most systems explored to date are *para*-oriented molecules (including Disperse Yellow 7 (DY7), Figure 1), which behave as one large conjugated photosystem.[24] Given

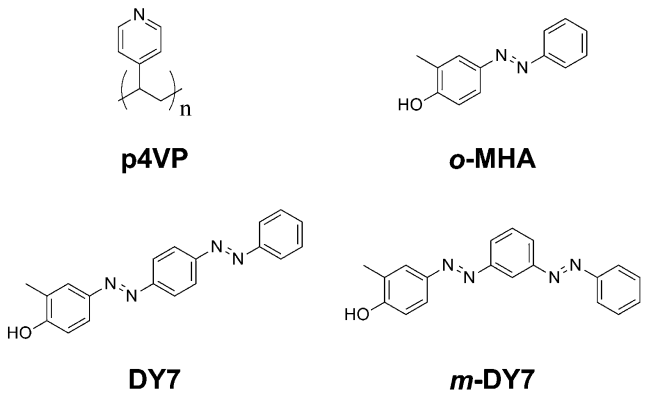

Figure 1. Structures of the studied compounds.

the success of DY7 in SRG formation,[29] we wanted to investigate the benefits of breaking this conjugation and gaining a system with two decoupled, potentially separately addressable isomerizing units. To achieve this, we designed and synthesized a new bisazo photosystem with the second azobenzene group oriented *meta* to the first (*m*-DY7, Figure 1). The placement of the second azobenzene in a *meta* position relative to the first in *m*-DY7 splits the bisazobenzene structure into two electronically independent azo units. To help elucidate the behavior of DY7 and *m*-DY7 and the consequences of this electronic independence, *ortho*-methyl hydroxy azobenzene (*o*-MHA, Figure 1) was used as a monoazo reference because the structure of the bonding unit to p4VP is similar to *o*-MHA in both bisazo dyes. We chose a noncovalent functionalization strategy, employing a supramolecular hydrogen-bonding approach to form complexes with the phenolic OH proton and the electron lone-pair of pyridine in p4VP. This allows for comparative studies on these chromophores which can all be bound to the same polymer.[29] Using this supramolecular approach provides batch-to-batch reproducibility of molecular weight and polydispersity among all the samples studied.

EXPERIMENTAL SECTION

Synthesis of *o*-MHA and *m*-DY7. ^{1}H NMR spectra were acquired at 300 K, on a Varian-Mercury 300 or 400 MHz spectrometer with ^{13}C NMR spectra being acquired on a Varian-Mercury 300 MHz NMR. Chemical shifts are reported in ppm on the δ scale using the solvent signal for reference. High resolution mass spectrometry (HR-MS) was acquired on a Thermo Scientific Exactive Plus Orbitrap. Samples were ionized using either atmospheric pressure chemical ionization (APCI) or electrospray ionization (ESI). All observed ions in positive and negative ionization modes are reported. All chemicals were obtained from Sigma-Aldrich Corporation and were used without further purification.

Synthesis of o-MHA, 2-Methyl-4-(phenyldiazenyl)phenol.[31] In a 100 mL round-bottom flask equipped with a stir bar, 15 mL of water and 15 mL of acetone was set to cool in an ice bath. Once the solvent temperature was below 5 °C, 456 μL of aniline (5 mmol, 1 equiv) was added followed by 0.414 g of $NaNO_2$ (6 mmol, 1.2 equiv) and 2.8 mL of 5 M HCl added dropwise (14 mmol, 2.8 equiv). The solution was left to stir for 30 min to diazotize the aniline, while in a second 250 mL round-bottom flask equipped with a stir bar, 40 mL of water and 20 mL of acetone was set to cool in an ice bath. To this second flask, 515 μL of ortho-cresol (5 mmol, 1 equiv), 1.06 g of Na_2CO_3 (10 mmol, 2 equiv), and 0.8 g of NaOH (20 mmol, 4 equiv) were added and set to stir in an ice bath to cool to below 5 °C. After the 30 min preactivation of the aniline, the contents of the first flask were added slowly to the second flask and left to stir for a further hour. After this time, the reaction mixture was extracted with 150 mL of ethyl acetate. The red organic phase was washed twice with 200 mL of water and then once with 100 mL of brine. The organic phase was dried with $MgSO_4$, filtered, and evaporated. The crude product was purified by silica column chromatography using a gradient of 0−30% ethyl acetate in hexanes. Dark orange crystals. Yield: 0.148 g, 14%.

^{1}H NMR (300 MHz, chloroform-*d*) δ, ppm: 7.88 (d, J = 7.03 Hz, 1 H), 7.71−7.79 (m, 2 H), 7.41−7.53 (m, 3 H), 6.87 (d, J = 8.50 Hz, 1 H), 5.38 (br. s., 1 H), 2.34 (s, 3 H).

^{13}C NMR (300 MHz, chloroform-*d*) δ, ppm: 156.8, 152.7, 146.9, 130.3, 129.1, 125.4, 124.7, 123.3, 122.5, 115.3, 15.9.

HR-MS (APCI, 4 kV) m/z: $[M + H]^+$ calcd for $C_{13}H_{13}N_2O$, 213.1022; found, 213.1020.

Synthesis of 1-(3-Nitrophenyl)-2-phenyldiazene.[32] In a 30 mL vial equipped with a stir bar, 0.365 g of nitrosoaniline (3.4 mmol, 1 equiv) was added followed by 0.602 g of 3-nitroaniline (4.4 mmol, 1.3 equiv). The blend was dissolved to a clear green solution with 15 mL of acetic acid and set to stir for 7 days, as it slowly turned orange. The product was purified by adding the acid solution to a separatory funnel with 80 mL of ethyl acetate and 300 mL of water. The red organic phase was washed twice with 200 mL of water and then once with 100 mL of brine. The organic phase was dried with $MgSO_4$, filtered, and evaporated. The crude product was purified by silica column chromatography using a gradient of 0−30% ethyl acetate in hexanes. Yellow crystals. Yield: 0.638 g, 83%.

^{1}H NMR (300 MHz, chloroform-*d*) δ, ppm: 8.69 (t, J = 2.05 Hz, 1 H), 8.28 (ddd, J = 8.12, 2.27, 1.02 Hz, 1 H), 8.19−8.25 (m, 1 H), 7.88−8.00 (m, 2 H), 7.66 (t, J = 8.05 Hz, 1 H), 7.49−7.58 (m, 3 H).

^{13}C NMR (300 MHz, chloroform-*d*) δ, ppm: 152.9, 152.1, 149.0, 132.1, 129.9, 129.2, 129.2, 124.9, 123.3, 117.0.

HR-MS (APCI, 4 kV) m/z: $[M]^+$ calcd for $C_{12}H_9N_3O_2$, 250.0587; found, 250.0597.

Synthesis of 3-(phenyldiazenyl)aniline.[33] In a 250 mL round-bottom flask equipped with a stir bar, 0.5 g of 1-(3-nitrophenyl)-2-phenyldiazene (2.2 mmol, 1 equiv) was added followed by 3.97 g of $Na_2S{\cdot}9H_2O$ (16.5 mmol, 7.5 equiv). The blend was dissolved in 54 mL of dioxane, 14 mL of ethanol and 3.5 mL of water and set to reflux at 90 °C for 4 h. The product was purified by adding the solution to a separatory funnel with 100 mL of ethyl acetate and 300 mL of water. The red organic phase was washed twice with 200 mL of water and then once with 100 mL of brine. The organic phase was dried with $MgSO_4$, filtered, and evaporated. The crude product was purified by

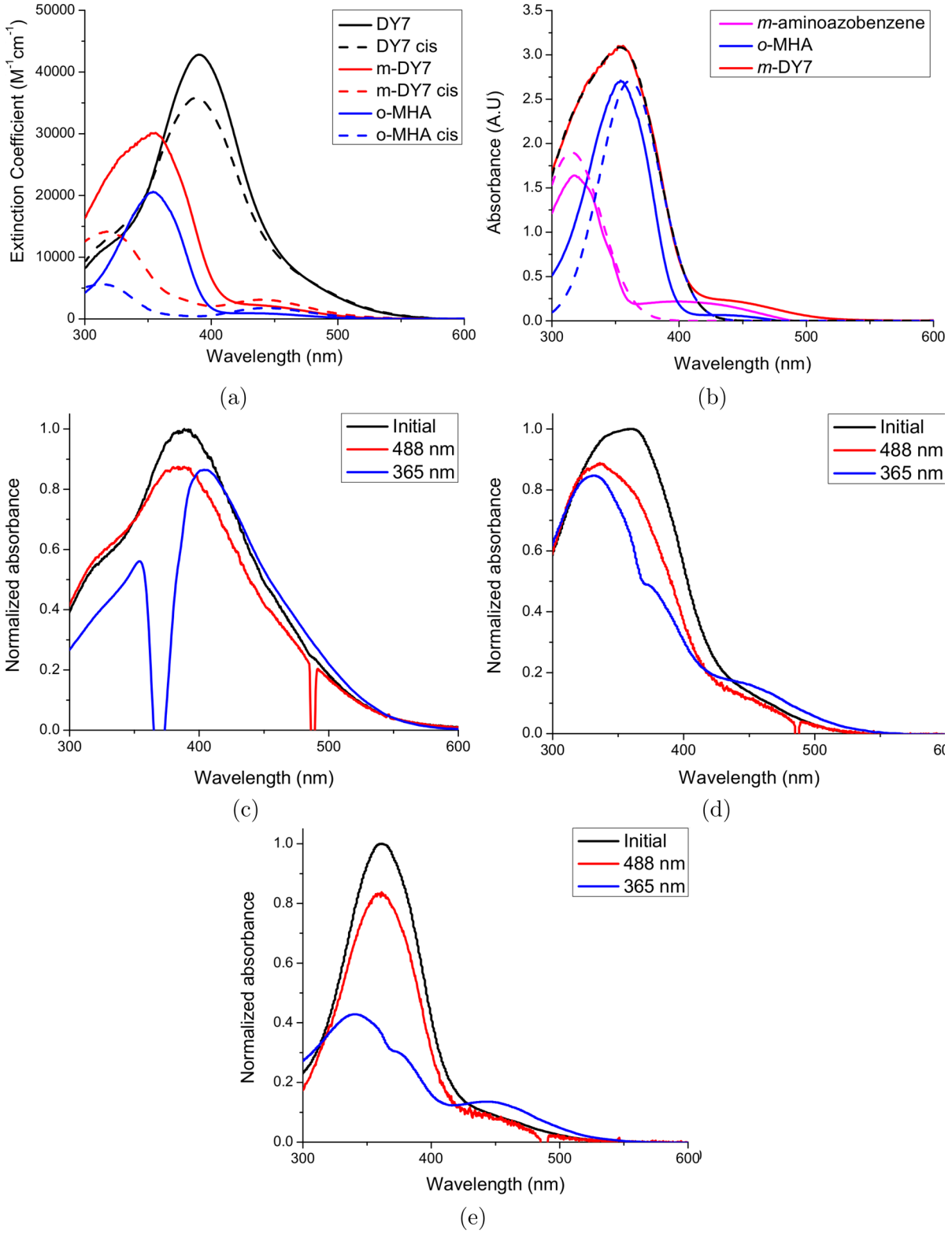

Figure 2. (a) UV−vis spectra of DY7, *m*-DY7, and *o*-MHA in THF. (b) Fitting of the *m*-DY7 spectrum with two gaussians and comparison to the spectra of *o*-MHA and 3-aminoazobenzene; spectra of (c) p(DY7), (d) p(*m*-DY7), and (e) p(*o*-MHA) in thin films in the dark and under illumination of 365 and 488 nm. The strong peaks evident particularly in (c) result from scattering of the pump light into the spectrometer.

silica column chromatography using a gradient of 0−50% ethyl acetate in hexanes. Red solid. Yield: 0.289 g, 67%.

^{1}H NMR (300 MHz, chloroform-*d*) δ, ppm: 7.87−8.02 (m, 2 H), 7.47−7.58 (m, 3 H), 7.41 (dt, J = 7.90, 1.17 Hz, 1 H), 7.33 (t, J = 7.75 Hz, 1 H), 7.20−7.28 (m, 1 H), 6.81 (ddd, J = 7.75, 2.34, 1.02 Hz, 1 H), 3.79 (br. s., 2 H).

^{13}C NMR (300 MHz, chloroform-*d*) δ, ppm: 153.8, 152.7, 147.3, 130.9, 129.9, 129.1, 122.8, 117.9, 115.0, 107.4.

HR-MS (ESI, 4 kV) m/z: $[M + H]^+$ calcd for $C_{12}H_{12}N_3$, 198.1026; found, 198.1023.

Synthesis of m-DY7, 2-Methyl-4-((3-(phenyldiazenyl)phenyl)-diazenyl)phenol.[31] In a 100 mL round-bottom flask equipped with

a stir bar, 40 mL of water and 20 mL of acetone was set to cool in an ice bath. Once the solvent temperature was below 5 °C, 0.289 g of 3-(phenyldiazenyl)aniline (1.45 mmol, 1 equiv) was added followed by 0.12 g of $NaNO_2$ (1.75 mmol, 1.2 equiv) and 2 mL of 2 M HCl was added dropwise (4 mmol, 4 equiv). The solution was left to stir for 30 min to diazotize the aniline, while in a second 250 mL round-bottom flask equipped with a stir bar, 40 mL of water and 20 mL of acetone was set to cool in an ice bath. To this second flask, 150 μL of ortho-cresol (1.45 mmol, 1 equiv), 0.120 g of Na_2CO_3 (3 mmol, 2.1 equiv), and 0.318 g of NaOH (6 mmol, 4 equiv) were added and set to stir in an ice bath to cool to below 5 °C. After the 30 min preactivation of the 3-(phenyldiazenyl)aniline, the contents of the first flask were slowly added to the second flask and left to stir for a further hour. After this time, the reaction mixture was extracted with 150 mL of ethyl acetate. The red organic phase was washed twice with 200 mL of water and then once with 100 mL of brine. The organic phase was dried with $MgSO_4$, filtered, and evaporated. The crude product was purified by silica column chromatography using a gradient of 0−40% ethyl acetate in hexanes. Dark orange solid. Yield: 0.184 g, 40%.

^{1}H NMR (300 MHz, chloroform-*d*) δ, ppm: 8.40 (d, J = 2.05 Hz, 1 H), 7.93−8.06 (m, 3 H), 7.81 (s, 1 H), 7.77 (dd, J = 8.49, 2.34 Hz, 1 H), 7.65 (d, J = 7.90 Hz, 1 H), 7.44−7.60 (m, 3 H), 6.89 (d, J = 8.49 Hz, 1 H), 5.55 (br. s., 1 H), 2.34 (s, 3 H).

^{13}C NMR (300 MHz, chloroform-*d*) δ, ppm: 157.0, 153.5, 153.4, 152.6, 146.9, 131.3, 129.6, 129.1, 129.1, 125.5, 125.1, 124.7, 124.6, 123.5, 123.0, 120.7, 116.0, 115.3, 15.9.

HR-MS (ESI, 4 kV) m/z: $[M - H]^-$ calcd for $C_{19}H_{15}N_4O$, 315.1252; found, 315.1251.

Kinetic Studies in Solution. A known mass of all small molecules were optically characterized by dissolving in a volumetric flask in dry spectral grade THF. The absorbance spectra were recorded on Cary Bio 300 UV/vis spectrophotometer. Solution-based kinetic data were recorded on the same instrument after irradiating the sample with a 405 nm diode laser with an intensity of 11 mW/cm^2 for 6 min, after which time all samples had achieved their photostationary states. The time-dependent rise in absorbance was tracked at the λ_{max} of the *trans* state, giving rise to a first order exponential growth of the *trans* state.

Preparation of the Thin Film Samples. Poly(4-vinylpyridine) (p4VP, Polymer Source, Inc., M_n = 3200 g/mol, M_w = 3800 g/mol), Disperse Yellow 7 (DY7, Sigma-Aldrich, 95%), as well as the synthesized *m*-DY7 and *o*-MHA were separately dissolved in tetrahydrofuran (THF, Sigma-Aldrich, >99.9%) and stirred for 2 h. Polymer−azobenzene complexes p(DY7), p(*m*-DY7), and p(*o*-MHA), with a nominal mixing ratio of 0.5 chromophores per polymer repeat unit, were prepared by mixing the requisite amount of polymer and dye stock solutions and stirring these complexed solutions for 2 h before spin-coating. SRG inscription was performed on spin-coated thin films (1000 rpm for 60 s) on clean microscope slides. UV−vis studies were carried out on thin films spin-cast on quartz glass from 2 wt % complex solutions, whereas SRG studies were conducted with samples from 4 wt % solutions. Film thicknesses were measured with a DEKTAK 6 M surface profiler.

UV−Vis Studies on Thin Films. The UV−vis spectra of thin films were measured in the dark and under irradiation with a fiber-optic spectrometer (Ocean Optics USB2000+). The illumination wavelengths were 365 nm (Thorlabs M365L2) and 488 nm (circularly polarized light from Coherent Innova 70 Argon-ion laser). To study *cis* isomer half-lives in the solid state, films were first pumped to the *cis* state (365 nm) and the thermal *cis*−*trans* relaxation was monitored by measuring the transmittance of a weak probe beam (390 ± 5 nm) obtained from a band-pass filtered, fiber-coupled Xenon light source (Abet Technologies LS150). To improve the signal-to-noise ratio, the probe was chopped at 200 Hz frequency and data was collected through a lock-in amplifier (Stanford Research Systems Model SR830 DSP).

Birefringence Studies. Photo-orientation was performed by exciting the chromophores with linearly polarized 365 and 488 nm light and measured by following the transmission of 820 nm diode laser through a polarizer−sample−analyzer configuration. The direction of the pump beam was set to ±45 degs with respect to the transmission direction of the polarizer/analyzer, and the birefringence values (Δn) were calculated from

$$I = I_0 \sin^2 \frac{\pi |\Delta n| d}{\lambda} \quad (1)$$

in which I stands for measured transmitted intensity, I_0 for transmitted intensity of the parallel polarizers setup prior to starting the writing process, d for the thickness of the film, and λ for the wavelength of the measuring beam.

Surface Patterning Studies. The surface-relief grating inscription was performed using circularly polarized light with a wavelength of 488 nm from a Coherent Innova 70 Ar^+ laser with an intensity of 300 mW/cm^2. The grating patterns were inscribed on the thin film samples using a Lloyd mirror interferometer setup, in which half of the incident beam hits directly the sample and the other half is reflected to the surface from a mirror perpendicular to the sample. The period of the resulting interference pattern can be tuned by changing the angle between the inscription beam and the sample normal. In this study, an angle of 13° was used in order to produce a grating with a 1 μm period.

The formation of the SRGs was monitored in real time by measuring the first-order diffraction efficiency of a horizontally polarized probe beam from a 635 nm diode laser with a photodiode as a function of time. The diffraction efficiency was calculated by dividing the power of the diffracted beam by the power of the same beam transmitted through the sample before the SRG inscription. The surface profiles of the inscribed gratings were characterized using a Veeco Dimension 5000 atomic-force microscope (AFM), with images of the SRGs being acquired two weeks after inscription.

RESULTS AND DISCUSSION

UV−Visible Spectroscopy and Photoisomerization. Figure 2a presents the UV−visible spectra of DY7, *m*-DY7, and *o*-MHA in THF both before (all-*trans* state) and after (photostationary state) illumination with a 405 nm laser. The initial spectra of *m*-DY7 and *o*-MHA show absorption maxima at 356 and 354 nm, respectively, being blue-shifted ∼35 nm as compared to the absorption maximum of DY7, measured at 390 nm. This is due to the longer conjugation length in DY7, which increases the delocalization of the π-electrons and thus lowers the energy of the $\pi-\pi^*$ transition.[34] Additionally, due to the hypsochromic shift of the $\pi-\pi^*$ transition in *m*-DY7 and *o*-MHA as compared to DY7, the low-intensity n-π^* absorption band around 440 nm is visible in these traces. Figure 2b shows that the absorption spectrum of *m*-DY7 can be fitted with two Gaussians, centered at 316 and 361 nm, indicating that the *meta*-substitution geometry electronically decouples the two azobenzenes units. By comparing the Gaussian fits to the spectra of *o*-MHA (λ_{max} 354 nm) and 3-aminoazobenzene (λ_{max} 318 nm) as model compounds for the two azobenzenes constituting *m*-DY7, we note that the Gaussian at 361 nm can be assigned to the OH-capped azo and 316 nm to the H-capped azo of the *m*-DY7. The absorbance at 440 nm results from the combination of the $n-\pi^*$ transitions of both azobenzene units.

In order to gain insight into the achievable photoconversion yield of the chromophores in solution, we studied their spectral changes upon irradiation (Figure 2a). The minimum *cis* content can be obtained by taking the ratio of the λ_{max} absorption of the photostationary state over the all-*trans* state. This does not preclude a residual *cis* absorption; however, this remains the simplest method to compare solution and film data, and as such, the photoconversion yield in all cases refers to a minimum *cis* yield. The photostationary state of DY7 is dissimilar compared to those of *m*-DY7 and *o*-MHA, in which a

significant decrease in the $\pi-\pi^*$ transition (minimum photoconversion yields being 78% and 96%, respectively) and a concomitant rise in absorbance of the $n-\pi^*$ transition at around 445 nm is observed. The spectral characteristics of the latter two are similar to the photochemical properties of the 4-hydroxy-substituted azobenzenes, as reported previously by Brode and colleagues.[35] Conversely, the photostationary state of DY7 simply decreases the intensity of $\pi-\pi^*$ absorption band at 390 nm (by 16%) with no evident changes in the shape of the spectrum.

In terms of potential photonic applications, it is pertinent to study the photochemical properties of the azobenzene units in thin polymeric films. Hydrogen bonding of alcohol-functionalized azobenzenes to the amine lone-pair electrons of poly(4-vinylpyridine) is an easy and versatile way of controlling azobenzene doping in the solid state without harmful chromophore−chromophore aggregation destroying the photonic properties.[6,29,36−39] On the basis of earlier studies, a mixing ratio of 50 mol % was selected as this ratio combines the high mass percentage of photoactive units in the material while still providing enough free volume, prohibiting hindered isomerization.[29] Figures 2c−e show the spectra of the thin films of the three studied compounds as complexed to p4VP and the spectral changes under illumination with 365 or 488 nm light. Although the spectral maxima have red-shifted a few nanometers and broadened (Table 1), similar initial spectral features as observed in THF are conserved in the solid state. We note that the minima at 365 nm and 488 nm in Figures 2c−e result from scattering of the pump light into the detector from the sample surface.

Table 1. Half-lives $T_{1/2}$, Maximum Absorption Wavelengths λ_{max}, and Minimum Photoconversion Yields γ for the Chromophores in THF and Polymer−Chromophore Complexes in Thin Films[a]

chromophore	DY7	*m*-DY7	*o*-MHA
$T_{1/2}$ in THF (min)	5.83	162.9	266.6
λ_{max} in THF (nm)	390	356	354
$T_{1/2}$, thin film (min)	2.60	8.80	6.50
λ_{max}, thin films (nm)	391	361	361
γ_{405}(%) in THF	15.5	78.0	95.9
γ_{365} (%), thin film	13.3	38.0	63.3
γ_{488} (%), thin film	12.6	17.9	17.1

[a]Minimum photoconversion yield is calculated from the maximum *trans* content at the photostationary state at a given irradiation wavelength.

The solid-state absorption spectra under illumination with 365 and 488 nm further highlight the differences of p(*m*-DY7) and p(*o*-MHA) as compared to p(DY7). As the former systems show separated $\pi-\pi^*$ and $n-\pi^*$ bands, we can address these transitions separately with 365 or 488 nm light. Figures 2d and e illustrate the photoconversion yields obtained for p(*m*-DY7) and p(*o*-MHA). When illuminating at 365 nm, although lower than when illuminating by 405 nm in THF solution, the photoconversion remains significant, whereas for 488 nm illumination the photoconversion yield remains below 20%. This demonstrates that for those two systems, we can easily tweak the photoinduced properties by changing the wavelength of the photoisomerizing light. As illustrated in Figure 2c, the spectral changes in p(DY7) are independent of the irradiation wavelength, both 365 and 488 nm result in a modest photoconversion yield of 13%. In general, we relate this low photoconversion, observed both in thin films and in solution, to the reduced quantum yield seen in *para*-conjugated bisazobenzenes.[24]

In measuring the *cis*-state decay in THF solution (Table 1), we observed that the half-life of DY7 is on a time scale of minutes, whereas the *cis* half-lives of *o*-MHA and *m*-DY7 are measured in hours, indicating that the *cis* isomer for the latter dyes is much more stable than that of DY7. These thermal decay kinetics in solution are of first order for all dyes, including the bisazomolecules DY7 and *m*-DY7, suggesting that there are no thermal isomerizations of both azo ends occurring at the same time. Given the qualitatively similar spectral changes upon irradiation in *m*-DY7 and *o*-MHA in THF as well as between the thin films of p(*m*-DY7) and p(*o*-MHA), the photoconversion in *m*-DY7 is likely to occur predominantly in the OH-capped azo portion of the molecule. Although the isomerizing azo unit is the same for *m*-DY7 and *o*-MHA, the shorter *cis* lifetime of the former can be related to more sterically hindered *cis* state of the *m*-DY7 as compared to *o*-MHA. When the supramolecular complex of these hydrogen-bonded dyes are spin-cast and annealed to a solid state, we observe a shortening of the *cis* lifetimes of all studied compounds. Individually, the effect of isomerization in a solid-state polymer matrix is much more drastic in *o*-MHA and *m*-DY7, bringing the *cis* lifetimes to the same order of magnitude with DY7 due to more constrained polymer environment surrounding them.

Material Testing. *Photo-Orientation.* Illuminating an azo-containing material with linearly polarized light leads to the buildup of photoinduced anisotropy, rendering the initially anisotropic materials birefringent.[40] Figure 3a presents the photoinduced birefringence as a function of time, the relaxation of the induced orientation after turning off the illumination, as well as the rerandomization of the molecular order under circularly polarized pump for all the studied complexes. Table 2 summarizes the obtained birefringence values and their long-term stability obtained by dividing the relaxed value by the saturated birefringence. Similar to spectroscopic studies, photo-orientation behavior of p(*m*-DY7) and p(*o*-MHA) is highly dependent on the irradiation wavelength as demonstrated by Figure 3b for p(*m*-DY7), whereas for p(DY7), birefringence can be inscribed in a similar qualitative fashion at both wavelengths.

The birefringence results can be rationalized as follows: as opposed to p(DY7), two different mechanisms producing photoinduced anisotropy can be identified for p(*m*-DY7) and p(*o*-MHA) depending on the irradiating wavelength. This is particularly evident in Figure 3b, which shows the difference in build-up for photo-orientation for p(*m*-DY7) when illuminated at 365 and at 488 nm. Illuminating that sample at 365 nm produces a high *cis*-isomer yield and, at the same time, does not drive efficient photoisomerization back to the all-*trans* state. A linearly polarized writing beam, thus, results in angularly dependent *cis*-concentration in the film (angular hole burning),[41,42] observed as relatively low saturated birefringence values and the fast saturation. In contrast, irradiation with 488 nm drives the photoisomerization in both directions for all the complexes, leading gradually to orientation of the molecular axis perpendicular to pump polarization resulting in higher birefringence values than the angular hole burning mechanism.[41,42] The wavelength-dependence of the dominant mechanism for p(*m*-DY7) and p(*o*-MHA) is evident also

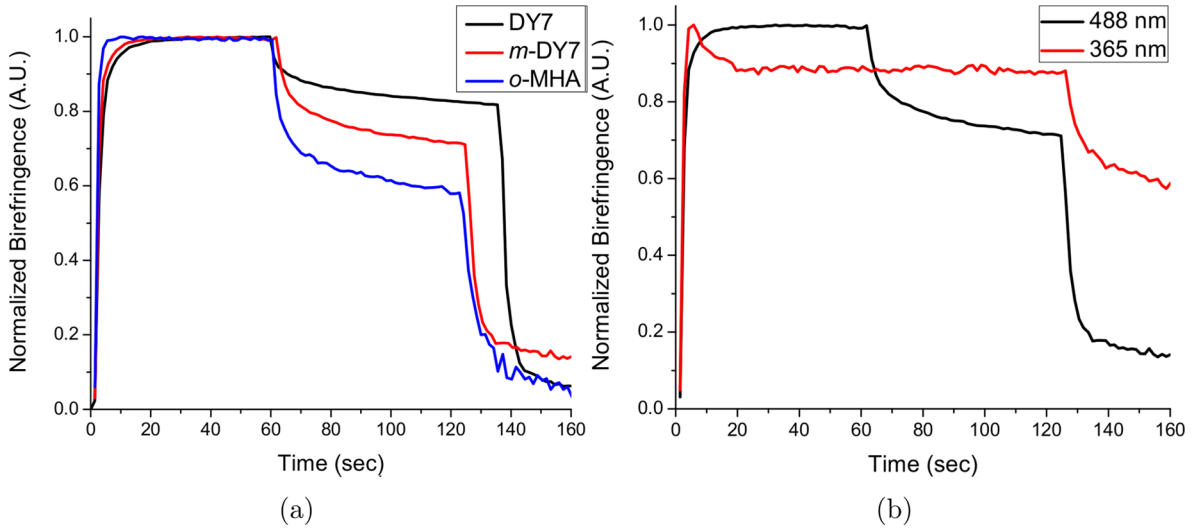

Figure 3. Normalized birefringence for thin films of (a) p(DY7), p(*m*-DY7), and p(*o*-MHA) inscribed at 488 nm light and for (b) p(*m*-DY7) at inscribed both at 365 and 488 nm light.

Table 2. Saturated Birefringence Values Δn and Their Long-Term Stability S in Thin Films of Polymer-Azobenzene Complexes of Thickness d As Inscribed at Different Wavelengths

sample	d (nm)	Δn_{488}	S_{488} (%)	Δn_{365}	S_{365} (%)
p(DY7)	195	0.035	82	0.017	74
p(*m*-DY7)	140	0.014	73	0.007	47
p(*o*-MHA)	170	0.008	59	0.004	21

based on the remnant birefringence values, being significantly less stable upon 365 nm irradiation, whereas the stability of p(DY7) is rather pump wavelength independent.

Upon irradiation with 488 nm, the build-up dynamics for birefringence is rather similar for all the compounds, rendering the comparison of photo-orientation efficiency more meaningful. We note that at this wavelength, the absorption coefficient of the materials is low, and even for p(DY7), the majority of the pump light propagates through the sample. It is interesting that for all the samples, this poorly absorbed pump light gives rise to higher birefringence than the 365 nm pump light, accentuating the fact that it is the *trans*−*cis*−*trans* cycling, as opposed to *trans*−*cis* isomerization, that drives the photo-orientation in amorphous azopolymers. When comparing the saturated birefringence values, they progress in the order of p(DY7) > p(*m*-DY7) > p(*o*-MHA). The fact that p(DY7), consisting of the rod-like DY7 molecules, results in the highest birefringence, which is over 2-fold the value of p(*m*-DY7) and over 4-fold the value of p(*o*-MHA), is to be expected based on its large aspect ratio.[26] Also, the larger size of *m*-DY7 chromophores as compared to *o*-MHA results in larger birefringence values. In this sense, using bisazobenzene chromophores provides additional advantage to photo-orientable materials.

The drop in the measured birefringence when irradiation is ceased (60s in Figure 3a) is due to (i) thermal back isomerization and (ii) thermal randomization of the anisotropic molecular alignment in the initially amorphous polymer systems. Because *cis* half-life for all the studied molecules in the solid state are similar, the long-term stability values measured on the order of several minutes remain comparable. Hence, it is clear that the angular diffusion of the

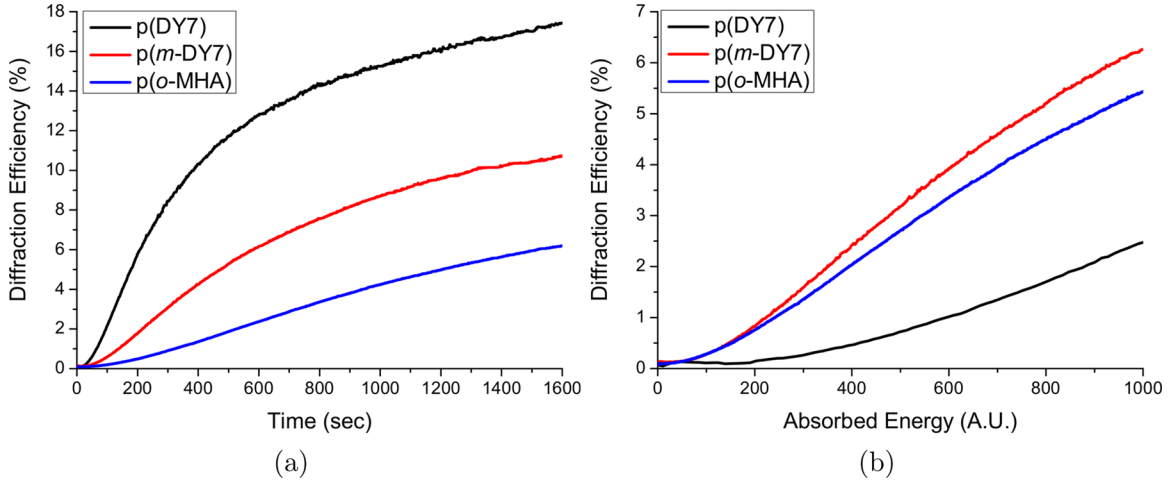

Figure 4. First-order diffraction efficiency upon SRG inscription at 488 nm light (a) as a function of time and (b) as a function of absorbed energy for thin films of polymer−azobenzene complexes.

bisazomolecules in p(DY7) and in p(*m*-DY7) upon thermal *cis*−*trans* relaxation is much lower than for the p(*o*-MHA). This is also supported by the fact that the buildup of birefringence for p(*o*-MHA) is remarkably faster than for the bisazobenzene complexes.

Meng and co-workers, as well as Cojocariu and co-workers linked the higher stability as well as slower buildup of birefringence in bisazochromophores to the idea that concurrent photoisomerization of both azo bonds is required to produce any motion of the chromophore with respect to its initial orientation.[26,34] Our results, as well as the results of Bléger and co-workers,[7,23] challenge this hypothesis because driving the bisazomolecules, especially the conjugated ones such as DY7 to *cis*−*cis* state, is very demanding. We address the higher stability (as well as the slower build-up kinetics) of the bisazochromophores to the steric hindrances that the longer-axis bisazo molecules face when reorienting upon thermal isomerization.

All-Optical Surface Patterning. When irradiating an azopolymer thin film with an interference pattern of two circularly polarized laser beams, the film deforms and forms a surface-relief pattern with the periodicity dictated by the light interference pattern. Figure 4a illustrates the growth of the first-order diffraction efficiency of the gratings upon SRG inscription at 488 nm. The original film thickness as well as final modulation depth of the gratings after an illumination of 1800 s at 300 mW/cm^2 are listed in Table 3. The SRG formation

Table 3. Obtained SRG Modulation Depths Λ after the Irradiation of 1800 s at 488 nm for Thin Films of Polymer−Azobenzene Complexes of Thickness *d*

sample	*d* (nm)	Λ (nm)
p(DY7)	340	315
p(*m*-DY7)	550	250
p(*o*-MHA)	620	170

efficiency at 488 nm develops in the order of p(DY7) > p(*m*-DY7) > p(*o*-MHA), the modulation depths of the gratings being 315, 250, and 170 nm, respectively. We note, however, that because p(DY7) has a much higher extinction coefficient at 488 nm than p(*m*-DY7) and p(*o*-MHA), the SRG formation in p(DY7) is driven by a remarkably larger number of photon absorptions than in the other studied materials.

A better way to consider SRG formation efficiency between materials with different optical densities is shown in Figure 4b, in which diffraction efficiency is plotted as a function of absorbed energy by the surface layer of the material. The energy, d*E*, absorbed during the time *t*, by a differentially thin layer of material, d*z*, having an area of *A* and when illuminated with an intensity I_{beam}, can be expressed by the equation

$$\frac{dE}{dz} = \alpha t A I_{beam} \quad (2)$$

in which α denotes the absorption coefficient of the material at the wavelength in question. Figure 4b shows the diffraction efficiency of all three complexes as a function of absorbed light, which gives the absorption-normalized SRG formation efficiency, and shows that in this comparison, p(DY7) is in fact the least efficient from the studied complexes. This is different from the non-normalized time-domain measurement (Figure 4a), in which p(DY7) was shown to be the most efficient. p(*m*-DY7), sharing the same azo unit than p(*o*-MHA), but comprising two azobenzene units, is shown to provide the most efficient SRG formation in this normalized comparison, indicating that a given light flux creates the largest material motions.

The higher SRG formation efficiency of p(*m*-DY7) as compared to p(*o*-MHA) can be rationalized by at least two factors. First, although it is in principle the same hydroxy-capped azo that is isomerizing in both *m*-DY7 and *o*-MHA, there is a possibility for the *m*-aminoazo head to act as an energy donor upon excitation, effectively increasing the isomerization yield of the hydroxyazobenzene of the bisazobenzene.[9,43] Second, the free-volume sweep upon photoisomerization of *m*-DY7 is larger than that of *o*-MHA creating more motion into the material. This follows previous reports that bulkier azobenzenes result in more efficient SRG formation in amorphous azo-polymers[44] and in molecular glasses.[45]

Most commonly, in SRG-forming amorphous azopolymers, push−pull-type azobenzenes with high absorption at blue-green wavelengths and high overlap of the $\pi-\pi^*$ and n-π^* bands are used.[22] p(*m*-DY7) and p(*o*-MHA), having well-separated $\pi-\pi^*$ and $n-\pi^*$ bands, are rather unconventional for SRG formation, yet they confirm that it is not the extent of initial absorption, but efficient *trans*−*cis*−*trans* cycling that is key to efficient SRG formation in the context of amorphous materials.[46] Because the initial absorption at writing wavelength, 488 nm, is already lower than at the $\pi-\pi^*$ absorption, the thickness of the films is not an issue and the films can, for example, be easily manipulated from the backside if needed. Although p(DY7) is more efficient in terms of absolute SRG formation efficiency, in terms of how efficiently the absorbed photons are transferred into mass transport of the polymer, p(m-DY7) is clearly superior to the conjugated p(DY7). We link this reduced performance to the lower photoconversion observed in both the solution state and thin films in these dyes.

■ CONCLUSIONS

We have demonstrated the power of rational molecular design for the buildup of fundamental understanding on light-responsive polymer materials. By varying between *meta*- and *para*-substitution of the second azobenzene in bisazobenzene molecules we show drastic differences in isomerization and thermal reconversion. In a materials context, namely, in the hydrogen-bonded polymer-azobenzene complexes, *meta*-substitution allows the two linked molecules to act independently allowing them to be addressed at different wavelengths, whereas the *para*-linkage causes the molecules to act as one large azo.

Highly conjugated *para*-substituted bisazobenzenes offer long aspect ratios and, thus, are seen as preferable for photo-orientation as compared to analogous monoazo derivatives. Changing the position of the additional azo unit to the *meta*-position, results in more efficient SRG formation than the corresponding monoazo. The photoinduced motions in azopolymers are dictated by the properties of the photoactive units and their interactions with the local environment. The supramolecular polymer-*meta*-bisazobenzene complexes are an attractive alternative for optimizing macromolecular motions in a manner that is far more optically transparent than current systems allowing for further progress in both the design of molecular chromophores as well as materials containing these switches.

AUTHOR INFORMATION

Corresponding Authors

*E-mail: jaana.vapaavuori@umontreal.ca.
*E-mail: alexis.goulet-hanssens@mail.mcgill.ca.

Present Addresses

[⊥]Department of Chemistry, Humboldt-Universität zu Berlin, Brook-Taylor-Straße 2, 12489 Berlin, Germany.
[#]Department of Chemistry and Bioengineering, Tampere University of Technology, P.O. Box 541, FI-33101 Tampere, Finland.

Author Contributions

[∥]J.V. and A.G.H. contributed equally to this work.

Notes

The authors declare no competing financial interest.

ACKNOWLEDGMENTS

J.V. is grateful for postdoctoral grant funded by Emil Aaltonen foundation. A.G.H. acknowledges FQRNT for a B2 doctoral scholarship as well as a B3 postdoctoral fellowship. A.P. acknowledges the financial support of Emil Aaltonen foundation. This work made use of the Aalto University Nanomicroscopy Center (Aalto-NMC) premises.

REFERENCES

(1) Theato, P.; Sumerlin, B. S.; O'Reilly, R. K.; Epps, T. H., III *Chem. Soc. Rev.* **2013**, *42*, 7055−7056.
(2) Dugave, C.; Demange, L. *Chem. Rev.* **2003**, *103*, 2475−2532.
(3) Russew, M.-M.; Hecht, S. *Adv. Mater.* **2010**, *22*, 3348−3360.
(4) Mahimwalla, Z.; Yager, K. G.; Mamiya, J.-I.; Shishido, A.; Priimagi, A.; Barrett, C. J. *Polym. Bull.* **2012**, *69*, 967−1006.
(5) Yu, H.; Ikeda, T. *Adv. Mater.* **2011**, *23*, 2149−2180.
(6) Priimagi, A.; Kaivola, M.; Virkki, M.; Rodríguez, F. J.; Kauranen, M. *J. Nonlinear Opt. Phys. Mater.* **2010**, *19*, 57−73.
(7) Bléger, D.; Dokic, J.; Peters, M. V.; Grubert, L.; Saalfrank, P.; Hecht, S. *J. Phys. Chem. B* **2011**, *115*, 9930−9940.
(8) Bléger, D.; Yu, Z.; Hecht, S. *Chem. Commun.* **2011**, *47*, 12260−12266.
(9) Yu, Z.; Hecht, S. *Angew. Chem., Int. Ed.* **2013**, *52*, 13740−13744.
(10) Bushuyev, O. S.; Tomberg, A.; Friščić, T.; Barrett, C. J. *J. Am. Chem. Soc.* **2013**, *135*, 12556−12559.
(11) Bushuyev, O. S.; Singleton, T. A.; Barrett, C. J. *Adv. Mater.* **2013**, *25*, 1796−1800.
(12) Hosono, N.; Kajitani, T.; Fukushima, T.; Ito, K.; Sasaki, S.; Takata, M.; Aida, T. *Science* **2010**, *330*, 808−811.
(13) Ikeda, T.; Ube, T. *Mater. Today* **2011**, *14*, 480−487.
(14) Lee, K. M.; Koerner, H.; Vaia, R. A.; Bunning, T. J.; White, T. J. *Soft Matter* **2011**, *7*, 4318−4324.
(15) Lee, K. M.; Smith, M. L.; Koerner, H.; Tabiryan, N.; Vaia, R. A.; Bunning, T. J.; White, T. J. *Adv. Funct. Mater.* **2011**, *21*, 2913−2918.
(16) Li, W.; Dohi, T.; Hara, M.; Nagano, S.; Haba, O.; Yonetake, K.; Seki, T. *Macromolecules* **2012**, *45*, 6618−6627.
(17) Haque, H. A.; Kakehi, S.; Hara, M.; Nagano, S.; Seki, T. *Langmuir* **2013**, *29*, 7571−7575.
(18) Iamsaard, S.; Aßhoff, S. J.; Matt, B.; Kudernac, T.; Cornelissen, J. J. L. M.; Fletcher, S. P.; Katsonis, N. *Nat. Chem.* **2014**, *6*, 229−235.
(19) Takaishi, K.; Muranaka, A.; Kawamoto, M.; Uchiyama, M. *J. Org. Chem.* **2011**, *76*, 7623−7628.
(20) Takaishi, K.; Muranaka, A.; Kawamoto, M.; Uchiyama, M. *Org. Lett.* **2012**, *14*, 276−279.
(21) White, T. J.; Tabiryan, N. V.; Serak, S. V.; Hrozhyk, U. A.; Tondiglia, V. P.; Koerner, H.; Vaia, R. A.; Bunning, T. J. *Soft Matter* **2008**, *4*, 1796−1798.
(22) Priimagi, A.; Shevchenko, A. *J. Polym. Sci., Part B: Polym. Phys.* **2014**, *52*, 163−182.
(23) Bléger, D.; Liebig, T.; Thiermann, R.; Maskos, M.; Rabe, J. P.; Hecht, S. *Angew. Chem., Int. Ed.* **2011**, *50*, 12559−12563.
(24) Cisnetti, F.; Ballardini, R.; Credi, A.; Gandolfi, M. T.; Masiero, S.; Negri, F.; Pieraccini, S.; Spada, G. P. *Chem.—Eur. J.* **2004**, *10*, 2011−2021.
(25) Robertus, J.; Reker, S. F.; Pijper, T. C.; Deuzeman, A.; Browne, W. R.; Feringa, B. L. *Phys. Chem. Chem. Phys.* **2012**, *14*, 4374−4382.
(26) Meng, X.; Natansohn, A.; Rochon, P. *Polymer* **1997**, *38*, 2677−2682.
(27) Wang, X.; Yin, J.; Wang, X. *Polymer* **2011**, *52*, 3344−3356.
(28) Wu, S.; Duan, S.; Lei, Z.; Su, W.; Zhang, Z.; Wang, K.; Zhang, Q. *J. Mater. Chem.* **2010**, *20*, 5202−5209.
(29) Vapaavuori, J.; Priimagi, A.; Kaivola, M. *J. Mater. Chem.* **2010**, *20*, 5260−5264.
(30) Koskela, J. E.; Vapaavuori, J.; Hautala, J.; Priimagi, A.; Faul, C. F. J.; Kaivola, M.; Ras, R. H. A. *J. Phys. Chem. C* **2012**, *116*, 2363−2370.
(31) Leriche, G.; Budin, G.; Brino, L.; Wagner, A. *Eur. J. Org. Chem.* **2010**, *2010*, 4360−4364.
(32) Asanuma, H.; Liang, X.; Komiyama, M. *Tetrahedron Lett.* **2000**, *41*, 1055−1058.
(33) Samanta, S.; Beharry, A. A.; Sadovski, O.; McCormick, T. M.; Babalhavaeji, A.; Tropepe, V.; Woolley, G. A. *J. Am. Chem. Soc.* **2013**, *135*, 9777−9784.
(34) Cojocariu, C.; Rochon, P. *Macromolecules* **2005**, *38*, 9526−9538.
(35) Brode, W.; Gould, J.; Wyman, G. *J. Am. Chem. Soc.* **1952**, *74*, 4641−4646.
(36) Priimagi, A.; Cattaneo, S.; Ras, R. H. A.; Valkama, S.; Ikkala, O. *Chem. Mater.* **2005**, *17*, 5798−5802.
(37) Priimagi, A.; Kaivola, M.; Rodriguez, F. J.; Kauranen, M. *Appl. Phys. Lett.* **2007**, *90*, 121103.
(38) Priimagi, A.; Vapaavuori, J.; Rodriguez, F. J.; Faul, C. F. J.; Heino, M. T.; Ikkala, O.; Kauranen, M.; Kaivola, M. *Chem. Mater.* **2008**, *20*, 6358−6363.
(39) Vapaavuori, J.; Valtavirta, V.; Alasaarela, T.; Mamiya, J.-I.; Priimagi, A.; Shishido, A.; Kaivola, M. *J. Mater. Chem.* **2011**, *21*, 15437−15441.
(40) Natansohn, A.; Rochon, P. *Chem. Rev.* **2002**, *102*, 4139−4175.
(41) Sekkat, Z.; Wood, J.; Knoll, W. *J. Phys. Chem.* **1995**, 17226−17234.
(42) Dumont, M.; El Osman, A. *Chem. Phys.* **1999**, *245*, 437−462.
(43) Bandara, H. M. D.; Burdette, S. C. *Chem. Soc. Rev.* **2012**, *41*, 1809−1825.
(44) Barrett, C. J.; Natansohn, A. L.; Rochon, P. L. *J. Phys. Chem.* **1996**, *3654*, 8836−8842.
(45) Wang, X.; Yin, J.; Wang, X. *Langmuir* **2011**, *27*, 12666−12676.
(46) Goldenberg, L. M.; Gritsai, Y.; Stumpe, J. *J. Opt.* **2011**, *13*, 075601.